Three-Dimensional Hierarchical Plasmonic Nano-Architecture Enhanced Surface-Enhanced Raman Scattering Immunosensor for Cancer Biomarker Detection in Blood Plasma

Ming Li,[†] Scott K. Cushing,[†,‡] Jianming Zhang,[§] Savan Suri,[†] Rebecca Evans,[∥,#] William P. Petros,[⊥,#] Laura F. Gibson,[∥,#] Dongling Ma,[§] Yuxin Liu,[¶] and Nianqiang Wu[†,⊥,*]

[†]Department of Mechanical and Aerospace Engineering and [‡]Department of Physics, West Virginia University, Morgantown, West Virginia 26506-6106, United States, [§]Institut National de la Recherche Scientifique, INRS-Énergie, Matériaux et Télécommunications, 1650 Boulevard Lionel-Boulet, Varennes, Québec J3X 1S2, Canada, and [⊥]Department of Basic Pharmaceutical Sciences, [∥]Department of Microbiology, Immunology, and Cell Biology, [#]Alexander B. Osborn Hematopoietic Malignancy and Transplantation Program of the Mary Babb Randolph Cancer Center, and [¶]Lane Department of Computer Science and Electrical Engineering, West Virginia University, Morgantown, West Virginia 26506, United States

ABSTRACT A three-dimensional (3D) hierarchical plasmonic nano-architecture has been designed for a sensitive surface-enhanced Raman scattering (SERS) immunosensor for protein biomarker detection. The capture antibody molecules are immobilized on a plasmonic gold triangle nanoarray pattern. On the other hand, the detection antibody molecules are linked to the gold nanostar@Raman reporter@silica sandwich nanoparticles. When protein biomarkers are present, the sandwich nanoparticles are captured over the gold triangle nanoarray, forming a confined 3D plasmonic field, leading to the enhanced electromagnetic field in intensity and in 3D space. As a result, the Raman reporter molecules are exposed to a high density of "hot spots", which amplifies the Raman signal remarkably, improving the sensitivity of the SERS immunosensor. This SERS immunosensor exhibits a wide linear range (0.1 pg/mL to 10 ng/mL) and a low limit of detection (7 fg/mL) toward human immunoglobulin G protein in the buffer solution. This biosensor has been successfully used for detection of the vascular endothelial growth factor in the human blood plasma from clinical breast cancer patient samples.

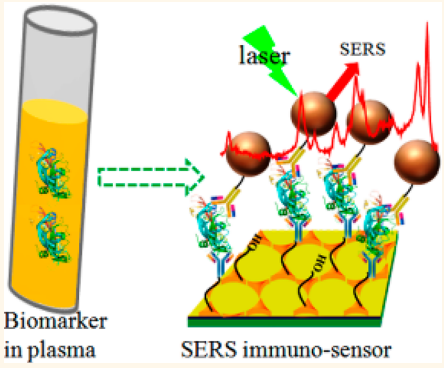

KEYWORDS: biosensor · biomarker · surface-enhanced Raman scattering · cancer · surface plasmon · blood plasma

Protein biomarkers are typically released from cells or organs, which are characteristic of physiologic and pathophysiologic conditions. Prompt monitoring of biomarkers holds great promise for early clinical diagnostics, which facilitates successful treatment of diseases and provides an optimal chance of affecting patient survival. Therefore, immunoassay techniques for biomarker measurement in complex biological samples are of fundamental importance to biomedical research and to diagnosis/prognosis of diseases.[1−3] Conventional approaches for biomarker measurement include the enzyme-linked immunosorbent assay (ELISA), radio-immunoassay, Western blot, and mass spectrometry.[4−8] These techniques are, however, complex, laboratory-based, time-consuming, and require experienced personnel to conduct the assay analysis. In addition, the blood serum concentrations of protein biomarkers associated with early stage cancers and infectious diseases generally range from 10^{-16} to 10^{-12} M.[9] However, commercially available immunoassays are typically capable of measuring proteins with a limit of detection (LOD) at the picomolar level,[10] which cannot optimally meet the critical need for protein detection. Moreover, these approaches cannot be used as a point-of-care (POC) technique for rapid,

* Address correspondence to nick.wu@mail.wvu.edu.

Received for review January 20, 2013 and accepted May 9, 2013.

Published online May 09, 2013
10.1021/nn4018284

high-throughput clinical diagnosis at low cost. Therefore, various biosensors have been developed toward POC testing of biomarkers, including fluorescent, electrochemical, and surface plasmon resonance (SPR) devices, *etc.*[11−16] However, the critical need for POC testing remains unmet, in part, because of the challenges in cost and interference from sample matrix background. Therefore, numerous efforts are being made to address these challenges, especially to develop sensors for rapid, accurate detection of biomarkers in real-world biological fluids (*i.e.*, urine, blood, serum, and plasma).[17−20]

Surface-enhanced Raman scattering (SERS) is emerging as a powerful analytical technique for chemical and biological sensing.[21−24] Compared with conventional immunoassays based on fluorescence, electrochemistry, and ELISA, SERS immunoassays have a lot of advantages.[25−27] For example, SERS provides the spectral fingerprint signatures of analytes, which endows SERS sensors with better anti-interference resistance to nonspecific molecules in the complex sample matrix as compared to electrochemical and fluorescent sensors. Moreover, it has the multiplexing detection capability with a single laser excitation due to its narrow-band Raman spectral signature and to its wide excitation wavelength. These unique attributes endow the SERS immunoassays ideal for biomarker detection in real-world biological samples. In general, SERS enhancement is attributed to electromagnetic (EM) enhancement and chemical enhancement (CE). The EM enhancement is typically much stronger than the CE enhancement. It is well-known that the EM enhancement is concentrated on the "hot spots", which are originated from the coupling of the localized surface plasmon resonance (LSPR) fields. Optimization of SERS substrate in size, shape, and composition is critical to the improvement in sensitivity and reproducibility of SERS assays.[28−31] Our previous studies have shown that the star shape of SERS substrate can concentrate the plasmonic field and create hot spots near the sharp tips due to the lightning-rod effect.[25] It is expected that the SERS substrates with a high density of sharp tips will provide high sensitivity for SERS sensing.[20,25,32] In addition, several studies have revealed that periodic and aperiodic nanostructures with the enhanced plasmonic field leads to strong SERS enhancement.[33−37] However, challenges still remain with the amplification of SERS signals due to the extremely small cross-section of Raman scattering.[38] In addition, the application of SERS sensors in clinical samples are still rare.

In the current study, a SERS immunosensor is constructed. The capture antibody is first immobilized on the gold triangle nanoarray chip. On the other hand, the detection antibody is conjugated with the SERS probe (Au@Raman reporter@SiO_2 sandwich nanoparticle). The antigen (analyte) is sandwiched between the capture antibody (linked to the nanoarray chip) and the detection antibody (conjugated to the SERS probe). This SERS sensor is characteristic of a three-dimensional (3D) hierarchical plasmonic nano-architecture, in which the Au nanostar@Raman reporter@SiO_2 sandwich nanoparticles are coupled to a periodic Au triangle nanoarray, generating a 3D plasmonic field. Under light excitation, a lot of hot spots are created between the triangles in the Au triangle nanoarray and also present between the sharp tips in the Au nanostars in the SERS probe. When many Au nanostar plasmonic antennas are brought close to the Au triangle nanoarray, high-density hot spots are generated in a 3D space. The resulting electromagnetic field is enhanced both in the space and in the intensity, which allows the Raman reporter molecules to experience the enhanced electromagnetic field, leading to remarkable amplification of the Raman signal of malachite green isothiocyanate (MGITC), the Raman reporter used. Based on this principle, the developed SERS immunosensor can be used for biomarker detection.

For comparative studies, three configurations of plasmonic nano-architectures are employed as the SERS substrates, including (i) the Au nanosphere@MGITC@SiO_2 particles coupled on a planar Au film, (ii) the Au nanosphere@MGITC@SiO_2 particles coupled on a Au triangle nanoarray, and (iii) the Au nanostar@MGITC@SiO_2 particles coupled on a Au triangle nanoarray. This allows us to investigate the effects of the Au chip (the planar Au film *versus* the Au triangle nanoarray) and the Au core (the Au sphere *versus* the Au star) on the performance of the SERS immunosensor. The three types of sensors are employed to detect the human immunoglobulin G (IgG) in the buffer solution. It is found that the Au nanostar/Au triangle nanoarray exhibits the highest sensitivity while the Au nanosphere/Au film is much less efficient. Therefore, the Au nanostar@MGITC@SiO_2/Au triangle nanoarray system is selected for detection of the vascular endothelial growth factor (VEGF) in human blood plasma of patients. VEGF is selected as the target analyte since it is a well-known protein biomarker for tumor-associated angiogenesis.[39−41] VEGF or its receptors are upregulated in several forms of human cancers. Targeting this protein with administration of a therapeutic antibody is approved by the FDA for treatment of selected malignancies.[39−41] In short, this work has demonstrated that the developed SERS immunosensor has great promise for detection of biomarkers in clinical blood plasma samples.

RESULTS AND DISCUSSION

Plasmonic Nanostructures and Their Conjugation with Antibody. When preparing the Au@MGITC@SiO_2 particles,[25] the MGITC molecules (Raman reporter) were first adsorbed onto the surface of Au core. A thin silica layer was then coated. As a result, the MGITC molecules were sandwiched between the Au core and the silica shell.

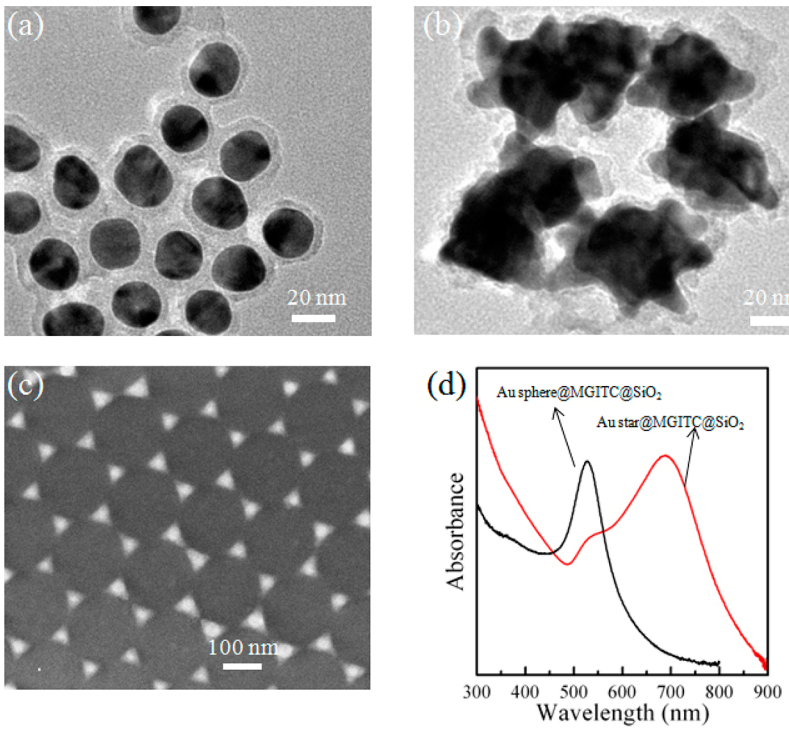

Figure 1. TEM images of the (a) Au sphere@MGITC@SiO_2 sandwich nanoparticles and (b) Au star@MGITC@SiO_2 sandwich nanoparticles. (c) SEM image of the Au triangle nanoarray, and (d) UV−visible absorption spectra of the Au sphere @MGITC@SiO_2 sandwich nanoparticles and the Au star@MGITC@SiO_2 sandwich nanoparticles.

The silica shell enables the SERS probe water-soluble and provides a platform for bioconjugation.[25,37] The plasmonic Au core is able to amplify the SERS signal.[25] The sandwich structure also prevents leaking of the Raman reporter molecules. In addition, many Raman reporter molecules are concentrated in a single sandwich nanoparticle as the SERS probe. As a result, the SERS signal results from a collection of Raman reporter molecules even for a single antibody−antigen binding event, which is an effective way to improve the sensitivity. Figure 1a,b shows the TEM images of the Au sphere@MGITC@SiO_2 and the Au star@MGITC@SiO_2 sandwich nanoparticles, respectively. It can be clearly seen that both the Au spheres and stars were coated with a 4−5 nm thick SiO_2 layer. Figure 1d shows the UV−visible absorption spectra of the Au sphere@MGITC@SiO_2 and the Au star@MGITC@SiO_2 sandwich nanoparticles. The Au sphere@MGITC@SiO_2 and Au star@MGITC@SiO_2 nanoparticles had the LSPR absorption bands at 520 and 690 nm, respectively. Also, the Au star@MGITC@SiO_2 nanoparticles exhibited a strong absorption shoulder at around 530 nm. The sandwich nanoparticles displayed strong SERS peaks of MGITC molecules, as shown in Figure S1 in the Supporting Information. The SERS signals from the Au star@MGITC@SiO_2 nanoparticles were much stronger than that from the Au sphere@MGITC@SiO_2 nanoparticles, which was due to greater plasmon-induced electromagnetic field enhancement in the Au stars.[25] The gap between the adjacent triangle corners in the Au triangle nanoarray was about 40 nm (Figure 1c). Such a small gap enabled the coupling of LSPR, generating a high density of hot spots for the SERS enhancement.

As shown in Figure 2a,b, the capture antibody and the detection antibody were conjugated to the nanoarray chip and the SERS probe (sandwich nanoparticle) by the carbodiimide chemistry,[20] respectively. It should be noted that the concentration of antibody solution applied in our protocols was quite high in order to ensure complete coverage of antibody on the substrate surface. Free excessive antibodies were removed by centrifugation and washing with the PBS buffer solution. The successful conjugation was confirmed by the FT-IR and XPS spectra (Figures S2 and S3).

Operating Principle of SERS Immunosensor. Figure 2c schematically represents the operating principle of the SERS immunosensor for biomarker detection. The SERS immunosensor is designed based on the sandwich-type configuration of antibody/antigen/antibody interaction. The SERS immunosensor included two processes performed in a humid chamber. First, the capture antibody-modified Au chip was immersed into a solution containing the analyte. During the incubation, the analyte (biomarker) bound to the capture antibody-modified Au triangle nanoarray chip. Excessive analyte was removed by washing with a PBS buffer solution. Next, the biomarker−antibody−Au nanoarray chip was incubated in a solution containing the Au

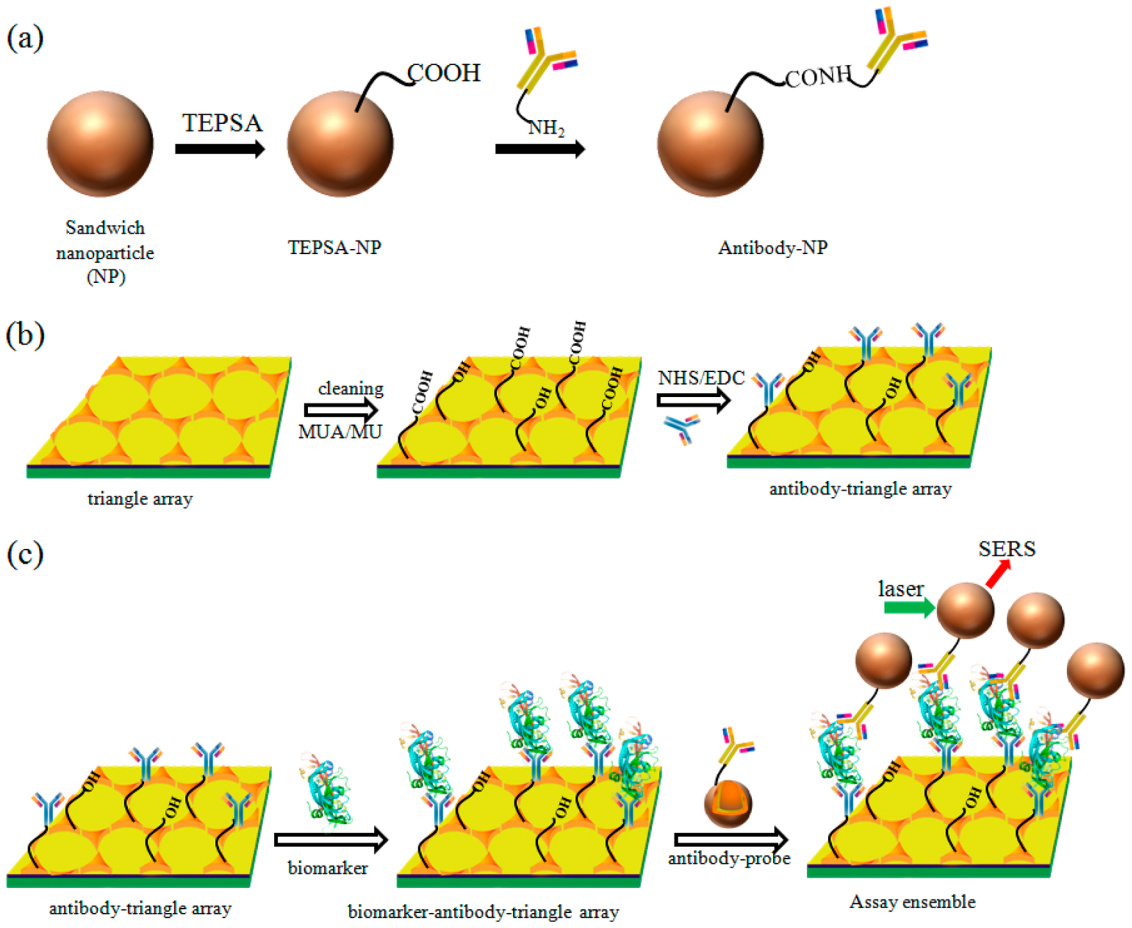

Figure 2. Schematic illustration of conjugation of the (a) SERS probe (sandwich nanoparticle) to the detection antibody and (b) Au triangle nanoarray chip to the capture antibody. (c) Schematic illustration of the operating principle of SERS immunosensor for biomarker detection. The structure of the VEGF biomarker is created by PyMOL with a four-digit code: 1VPF.

star@MGITC@SiO_2 nanoparticle conjugated with the detection antibody. Since the antigen (analyte) in the present work had at least two binding sites, it can bind to both the detection antibody and the capture antibody, leading to the formation of the nanoparticle/biomarker/chip sandwich architecture. After washing with a PBS buffer solution, the free sandwich nanoparticles were removed. Finally, the chips were illuminated with the laser, and the SERS signal from the MGITC was recorded.

Comparison of Immunosensor Performance in Various Sandwich Assemblies. In order to optimize the performance of the SERS immunosensor, three configurations of plasmonic nano-architectures were employed as the SERS substrates, including (i) the Au nanosphere@MGITC@SiO_2 particles coupled on the planar Au film, (ii) the Au nanosphere@MGITC@SiO_2 particles coupled on the Au triangle nanoarray, and (iii) the Au nanostar@MGITC@SiO_2 particles coupled on the Au triangle nanoarray. For the sake of optimization, IgG was selected as the protein analyte because the IgG and its antibodies are much less expensive than VEGF and its corresponding antibodies.

Figure 3 and Figure S4 show the SERS spectra of all three types of sensors that responded to various concentrations of IgG in the PBS buffer solution. The SERS intensity increased with an increase in the IgG concentration. The calibration curves were obtained by plotting the SERS peak intensity at 1578 cm^{-1} as a function of the IgG concentration (Figure 4). The Au nanostar@MGITC@SiO_2 particles on the Au triangle nanoarray showed the strongest SERS intensity at the corresponding IgG concentration in comparison with the Au sphere sandwich nanoparticle/Au film and the Au sphere sandwich nanoparticle/Au triangle nanoarray. The Au sphere sandwich nanoparticle/Au film displayed the lowest SERS response. Furthermore, the calibration curves showed 5−6 orders of magnitude dynamic linear ranges of the IgG concentration (Table 1). In the linear region, the calibration curves were fitted as $y = 270.90x + 295.29$ ($R^2 = 99.2\%$) for the Au sphere sandwich nanoparticle/Au film, $y = 488.64x + 221.15$ ($R^2 = 97.7\%$) for the Au sphere sandwich nanoparticle/Au triangle nanoarray, and $y = 1245.66x + 1251.88$ ($R^2 = 93.8\%$) for the Au star sandwich nanoparticle/Au triangle nanoarray. Here, y is the SERS intensity at

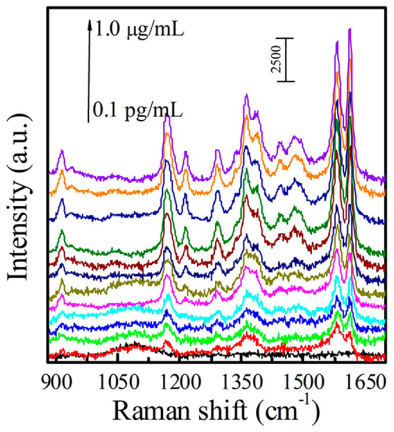

Figure 3. SERS spectra of the Au star@MGITC@SiO_2 sandwich nanoparticle coupled to the Au triangle nanoarray chip in various concentrations of IgG in the PBS buffer solution (0.1 pg/mL, 0.5 pg/mL, 1.0 pg/mL, 5.0 pg/mL, 10 pg/mL, 50 pg/mL, 0.1 ng/mL, 0.5 ng/mL, 1.0 ng/mL, 10 ng/mL, 100 ng/mL, 500 ng/mL, and 1.0 μg/mL).

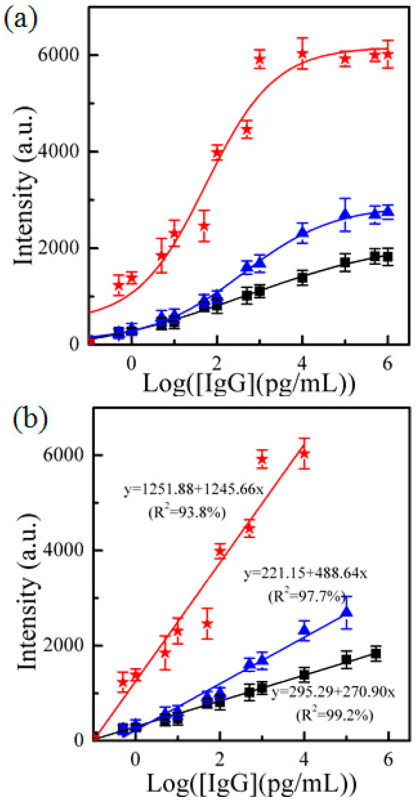

Figure 4. (a) Plots of SERS peak intensity at 1578 cm^{-1} as a function of the logarithmic concentration of IgG, and (b) the linear range of (a). Black box: Au sphere coupled on the Au film. Blue triangle: Au spheres coupled on the Au triangle nanoarray. Red star: Au stars coupled on the Au triangle nanoarray.

1578 cm^{-1}, and x is the logarithmic concentration of IgG (pg/mL). It should be noted that the highest sensitivity was achieved by the Au star sandwich nanoparticle/Au triangle nanoarray. In addition, the LOD was obtained on the basis of 3S/N.[42,43] The results showed that LOD was 45 ± 3 fg/mL for the Au sphere sandwich nanoparticle/Au film, 25 ± 5 fg/mL for the Au sphere sandwich nanoparticle/Au triangle nanoarray, and 7 ± 5 fg/mL for the Au star sandwich nanoparticle/Au triangle nanoarray. In short, the Au star sandwich nanoparticle/Au triangle nanoarray system exhibited the best performance in terms of LOD and sensitivity. Furthermore, the performance of the current SERS immunosensor was compared with those reported in the literature, including fluorescent, electrochemical, colorimetric, and SPR sensors, as listed in Table 2. It can be seen that the present sensor exhibited a lower LOD.

Three-Dimensional Electromagnetic Field Enhancement. FDTD simulations were used to explore the origin of the enhanced performance of the Au star/Au triangle array compared to the Au sphere/Au triangle array and the Au sphere/Au film sensor. Although the exact geometry of the Au sphere and star on the top of the triangle array cannot be simulated, the origin of the enhanced SERS can be explored by simulating multiple symmetric positions and examining the average enhancement (Figure S5). For the Au sphere/Au film, the coupled LSPR resulted in the SERS enhancement ($|E/E_0|^4$) of ~6400. When the Au spheres were coupled to the Au triangle nanoarray, the SERS enhancement ($|E/E_0|^4$) increased slightly to ~8000. The exact orientation of spheres on the triangle array was unknown, but Figure S5c shows that an increased EM field of varying strength existed regardless of position. Although the enhancement magnitude of the LSPR field increased slightly when the Au spheres were coupled to the triangle array instead of the film, the number of possible coupling positions increased greatly.

For the Au sphere/Au film sensor to have a measurable SERS signal, two spheres must attach to the Au film in proximity (Figure S5b). The spheres can attach at any position on the film, reducing the probability of coupling except for a high analyte level. In the Au sphere/Au triangle array, the spheres can only attach to the triangle array and not the surrounding area. This ensures a high probability of coupling and measurable SERS signal even at a low analyte concentration. The average SERS signal therefore increases for a given concentration when the Au film is replaced with the Au triangle array even if the LSPR peak is comparable. It should be noted that the Au triangle array alone had similar strength to the coupled Au sphere/Au triangle array (Figure S5a). This indicates that the LSPR field was primarily from the Au triangle and not from the Au sphere−Au triangle resonance at 532 nm.

Figure S5d shows the electromagnetic field for the Au star/Au triangle array. The SERS enhancement ($|E/E_0|^4$) was ~1 000 000, which was significantly higher than either the Au sphere/Au triangle array or the Au sphere/Au film. As shown in our previous work, the 532 nm LSPR mode was originated from coupling of

TABLE 1. Performance of SERS Immunosensors with Different Configurations

assay system	linear range (pg/mL)	sensitivity (slope of fitted curve)	LOD based on 3S/N (fg/mL)
Au sphere@MGITC@SiO_2 on Au film	$0.1-5.0 \times 10^5$	270.9	45 ± 3
Au sphere@MGITC@SiO_2 on Au triangle nanoarray	$0.5-1.0 \times 10^5$	488.6	25 ± 5
Au star@MGITC@SiO_2 on Au triangle nanoarray	$0.1-1.0 \times 10^4$	1245.7	7 ± 5

TABLE 2. Summary of Representative Sensors for Detection of IgG and VEGF

sensing system	sensing principle	biomarker	type of assay	linear range	LOD	refs
Au array	fluorescence	IgG	direct	1 μM ~ 1 fM	0.3 fM	44
Au/protein	electrochemical	IgG	direct	$10-10^4$ ng/mL	3 ng/mL	45
glass/Au	colorimetry	IgG	sandwich	1—5000 ng/mL	60 ng/mL	46
magnetic NPs	piezoelectricity	IgG	sandwich	0.6—34.9 μg/mL	0.36 μg/mL	47
Au/aptamer	voltammetry	VEGF	direct	50—150 pM	50 pM	48
carbon fiber microelectrode	voltammetry	VEGF	direct	10—100 pg/mL	38 pg/mL	49
SiO_2/protein	fluorescence	VEGF	direct	0—50 ng/mL	1.0 ng/mL	50
Au film	SPR	VEGF	direct	20—600 ng/mL	3 ng/mL	51

the spikes in the nanostar.[25] When the tip of the spike was brought near the triangle, further LSPR coupling occurred between the spikes and the triangle, increasing the SERS signal. The spike—triangle coupling increases the intensity and spatial extension of the local electromagnetic field. The enhanced area of electromagnetic field means that more Raman reporters were subject to the SERS enhancement. Although the exact shape of the star and their positions on the triangle array were unknown, the relatively large size and multiple spikes of the star ensured that strong coupling was present when attached to the triangle nanoarray (Figure S5d). Therefore, the 3D hierarchical architecture generated a high density of hot spots.

The enhanced SERS signal of the Au star/Au triangle array resulted from the increased strength, area, and probability of the LSPR coupling. In particular, the improved performance of the Au star/Au array sensor came from the increased probability of coupling between the capture and the signal structures. An effective way to improve the sensor performance is to use a large signal structure (nanostar) with multiple LSPR active features on the surface. This allows for a single capture event to create multiple points of increased SERS signal, which effectively allows one Au nanostar to act as several nanospheres while only requiring one signal analyte to be detected. This process allows the LOD to be further lowered.

Detection of VEGF in Clinical Blood Plasma Samples with the SERS Immunosensor. The above-mentioned results showed that Au nanostar coupled to the Au triangle nanoarray was the best SERS substrate. Hence the Au star@MGITC @SiO_2 sandwich nanoparticle/Au triangle nanoarray was selected for detecting VEGF in the human blood plasma. Before testing clinical samples, the SERS immunosensor was calibrated with known concentrations of VEGF spiked into blood plasma. Prior to addition of VEGF,

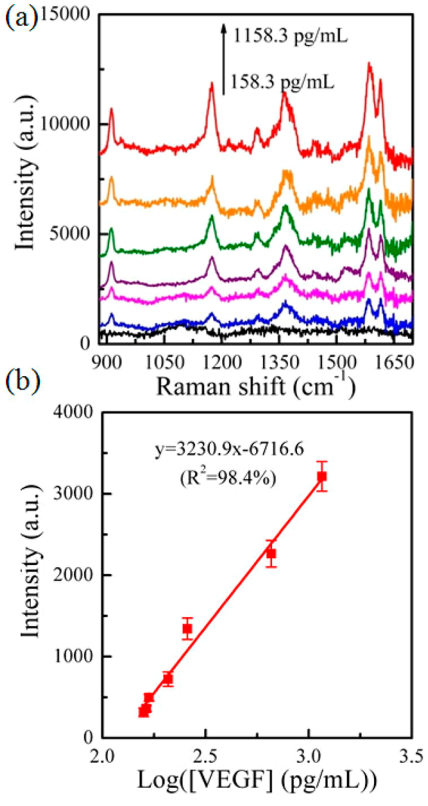

Figure 5. (a) SERS spectra of the Au star@MGITC@SiO_2 sandwich nanoparticle/Au triangle nanoarray immunosensor, which responded to various concentrations of VEGF biomarker in blood plasma, and (b) plot of the intensity of SERS peak at 1578 cm^{-1} as a function of the logarithmic concentration of VEGF in blood plasma.

the baseline concentration of VEGF in the blood plasma matrices was estimated by a validated commercial ELISA kit. Figure 5 shows the SERS spectra of the Au star sandwich nanoparticle/Au triangle nanoarray immunosensor system in the presence of various concentrations

TABLE 3. VEGF Concentration in Clinical Blood Plasma Samples Measured by Both the Developed SERS Immunosensor and a Standard ELISA Method

sample no.	[VEGF] *via* ELISA (pg/mL)	[VEGF] *via* SERS biosensor (pg/mL)
1	600.1 ± 12.6	585.9 ± 12.5
2	337.7 ± 14.6	301 ± 9.6
3	569.6 ± 6.9	588.8 ± 15.3

of VEGF in blood plasma. Obviously, the intensity of SERS peak at 1578 cm^{-1} gradually increased with an increase in the VEGF concentration. The calibration curve of the SERS peak intensity *versus* the logarithmic concentration of VEGF was fitted as $y = 3230.9x - 6716.6$, with the relative coefficient (R^2) of 98.4%, where y is the peak intensity at 1578 cm^{-1} and x is the logarithmic concentration of VEGF. The calibration curve indicated that our SERS assay system can work for VEGF detection in blood plasma.

After calibration, the developed SERS immunosensor was used for detection of VEGF in blood plasma from clinical samples of patients with breast cancer. The VEGF concentration in the same clinic samples was also measured using the standard ELISA method. Table 3 compared the mean VEGF concentration values measured by the SERS immunosensor and the ELISA for three unknown clinical samples. The results show a high degree of similarity, which suggested that the present SERS sensor was capable of detecting VEGF in clinical samples. Obviously, the SERS immunosensor provides significant advantages over the conventional ELISA approach. For example, robust detection in complex matrices, short detection time, fewer washing steps, and easy operation are evident with this novel approach.

CONCLUSIONS

In summary, an ultrasensitive SERS immunosensor was developed for protein biomarker detection. The sandwich nanoparticles conjugated with the detection antibody were coupled with a Au triangle nanoarray functionalized with the capture antibody *via* the protein biomarker. Coupling of the sandwich nanoparticle-based SERS probes with the Au triangle nanoarray created a 3D hierarchical architecture, forming a 3D confined plasmonic field. The resulting 3D plasmonic field was enhanced in intensity and in 3D space, which generated a high density of hot spots. Therefore, the Raman signal of the MGITC molecules embedded in the sandwich nanoparticles was greatly amplified. Furthermore, the sandwich nanoparticle−SERS probes containing the Au star core led to much higher sensitivity for the SERS immunosensor than the one with the Au sphere as the core, and the Au triangle nanoarray endowed much higher sensitivity than the planar Au film. The 3D FDTD simulation confirmed that the enhanced plasmonic field both in intensity and in space contributed to the high sensitivity of the SERS sensor. As a result, the developed SERS immunosensor was able to sensitively detect the protein biomarker with a wide dynamic linear range over several orders of magnitude. In addition, the present SERS immunosensor was capable of detecting the VEGF biomarker in clinical blood plasma samples. It is believed that the present SERS immunosensor can be further developed for point-of-care testing.

METHODS

Chemicals and Materials. Malachite green isothiocyanate (MGITC) was purchased from Molecular Probes, Inc. 3-Triethoxylsilylpropyl succinic anhydride (TEPSA) was purchased from Gelest Inc. Goat anti-human IgG polyclonal antibody, IgG from human serum, (3-aminopropyl)trimethoxysilane (APTMS), 5 M NaCl solution, and sodium silicate stock solution (26.5% SiO_2 in 10.6% Na_2O), *N*-hydroxysuccinimide (NHS), 1-ethyl-3-(3-dimethylaminopropyl)carbodiimide (EDC), 11-mercaptoundecanoic acid (MUA), and 11-mercapto-1-undecanol (MU) were purchased from Sigma-Aldrich. Na_2HPO_4 (99.0%) and NaH_2PO_4 (99.0%) came from Alfa Aesar. Human VEGF monoclonal antibody (capture antibody, cAb) and human $VEGF_{165}$ biotinylated polyclonal antibody (detection antibody, dAb) were purchased from R&D Systems, Inc. The planar gold film chips were purchased from EMF Corp. (Ithaca, NY). Deionized (DI) water was produced by a Milli-Q Millipore system (18.2 MΩ·cm, Millipore Corp., USA). All solvents were obtained from commercial sources and used without further purification. In addition, citrated blood samples were obtained from patients with breast cancer and control patients without cancer following written informed consent according to the West Virginia University Health Sciences Institutional Review Board guidelines.

Synthesis of Sandwich Nanoparticles and Its Conjugation with Detection Antibody. Au nanospheres and Au nanostars were synthesized according to our previous reports.[20,25] Briefly, Au sphere @MGITC@SiO_2 and Au star@MGITC@SiO_2 sandwich nanoparticles were prepared with the MGITC concentration of ~1.0×10^{-6} M.[20,25] The resulting sandwich nanoparticles were dissolved in 200 μL of phosphate buffered saline (PBS) (10 mM Na_2HPO_4/NaH_2PO_4, 0.3 M NaCl and pH 7.0) solution for further use. One hundred microliters of TEPSA was added into 100 μL of PBS solution of the sandwich nanoparticles (Au sphere@MGITC@SiO_2 or Au star@MGITC@SiO_2) obtained above and then incubated for 2 h to achieve the carboxyl-group-terminated sandwich nanoparticles. After being centrifuged and washed with the PBS buffer solution, the carboxyl group sandwich nanoparticles were incubated for 1 h in a PBS buffer solution containing 50 mM NHS and 200 mM EDC, followed by addition of 100 μL of 1.0 g/L detection antibody (anti-human IgG polyclonal or human $VEGF_{165}$ biotinylated polyclonal antibody) and incubation overnight. The solution was centrifuged and washed with a PBS buffer solution to remove free excess antibody, and then the resulting detection antibody sandwich nanoparticle conjugates were stored in 100 μL of PBS buffer solution for future use.

Gold Nanoarray Fabrication and Functionalization of Chips with Capture Antibody. The Au triangle nanoarray on a glass slide was fabricated using nanosphere lithography as shown in our previous reports.[52,53] A monolayer of hexagonally close-packed polystyrene spheres (200 nm in a diameter) was first self-assembled on a glass slide. A 10 nm thick titanium and a 50 nm thick Au layer were then deposited using e-beam evaporation. Subsequently, the chips were sonicated in ethanol to lift off the polystyrene spheres, leaving an array of Au triangles on the glass slide.

For surface functionalization, the chips (Au planar film and Au triangle nanoarray) were first cleaned by successive immersion in CH_2Cl_2, ethanol, and DI water each for 10 min, and then dried in a vacuum oven at 60 °C for 1 h. The cleaned chips were incubated overnight in an ethanolic solution containing 100 mM MUA and 100 mM MU and then washed with ethanol to remove free MUA and MU. The resulting MUA/MU-modified chips were activated by immersion in a PBS solution containing 50 mM NHS and 200 mM EDC. After being washed with a PBS buffer solution, chips were incubated overnight in a PBS buffer solution of 1.0 g/L capture antibody (anti-human IgG polyclonal or human VEGF monoclonal antibody), followed by rigorously washing with PBS buffer solution to remove free capture antibody and kept in a humid chamber prior to assay.

SERS Immunosensor. Two types of immunoassay experiments, the IgG immunoassay in a PBS buffer solution and the VEGF immunoassay in blood plasma, were conducted.

(a). IgG Immunoassay in PBS Buffer Solution. The SERS immunoassay was carried out in a two-step process. The anti-human IgG chip was first immersed into a solution of various IgG concentrations (0.1 pg/mL, 0.5 pg/mL, 1.0 pg/mL, 5.0 pg/mL, 10 pg/mL, 50 pg/mL, 0.1 ng/mL, 0.5 ng/mL, 1.0 ng/mL, 10 ng/mL, 100 ng/mL, 500 ng/mL, and 1.0 μg/mL), and after incubation for 20 min, the chip was vigorously rinsed with PBS to remove free IgG. Then, the chip was immersed into the solution of anti-human IgG sandwich nanoparticle conjugates and incubated for 10 min, followed by rinsing with PBS to remove free sandwich nanoparticles. The resulting sandwich nanoparticle@IgG@chip was subject to the SERS measurement.

(b). VEGF Immunoassay in Anticoagulant Human Blood Plasma. First, the baseline concentration of VEGF in human blood plasma was determined to be 158.3 pg/mL by a validated commercial ELISA kit (R&D Systems, Minneapolis, MN). The human blood plasma was spiked with the VEGF stock solution (1 ng/mL) in human blood plasma to achieve a standard curve, with an upper limit of 1.158 ng/mL. The concentration of VEGF in the plasma was measured with ELISA. Each of the three samples used were completed in triplicate for the ELISA.

For measurement of VEGF with the immunosensor, the cAb chip was incubated for 20 min in human blood plasma of various VEGF concentrations and then rinsed with PBS buffer solution to remove free VEGF and other molecules. Then, the VEGF-bound cAb chip was immersed into the solution of dAb sandwich nanoparticles obtained above and incubated for 10 min, followed by the same procedure as that for the IgG immunoassay to remove free sandwich nanoparticles. The resulting sandwich nanoparticle@VEGF@chip was subject to the SERS measurement. The resulting curve was used for the calibration curve of VEGF concentration. The measurement for clinical samples followed a similar procedure except for the replacement of VEGF solution.

Instrumentation. The Au triangle array chip was observed under a field-emission scanning electron microscopy (SEM, JEOL JSM-7600F). The structure of nanoparticles was observed with a transmission electron microscopy (TEM, JEOL JEM-2100F) at an acceleration voltage of 200 kV. UV−visible absorption spectra were acquired with a Shimadzu UV-2550 spectrometer. The chemical structure was measured with a Fourier transform infrared (FT-IR) spectrometer (Thermo Nicolet 6700) under the attenuated total reflection (ATR) mode and with a PHI 5000 Versa Probe X-ray photoelectron spectroscopy (XPS) system (Physical Electronics, MN). XPS spectra were calibrated with the reference to the C 1s peak at 284.8 eV. Raman spectra were obtained with a Renishaw InVia Raman spectrometer equipped with a 532 nm laser. Three SERS spectra were collected from different sites for each sample and then averaged to represent the SERS results. The maximum laser power on the sample, which was measured by a power meter (Newport, model 1918-R), was around 0.017 mW, and the accumulation time was 10 s.

Finite Difference Time Domain Simulation. Finite difference time domain (FDTD) simulations were performed using the open source MEEP code.[54] The dielectric function for Au was a series of four Lorentz sums fitted to the data of Johnson and Christy.[55] A background dielectric constant of 1.33 was used to replicate the liquid phase of the sensor. The Au triangle array and nanospheres used for simulations had identical dimensions to those shown in the SEM/TEM image (Figure 1a,c). The absorption spectrum of the Au nanospheres was matched to the experimental UV−visible measurement. The SiO_2 shell was found not to have a large impact on the simulation and was left out for computational simplicity. The Au nanostar's shape was approximated by a sphere of equal size to the core shown in the TEM image (Figure 1b), covered by an array of cones. The shape was an idealization of the synthesized nanostar which had a nonsymmetric random structure. The simulated and experimental Au nanostar absorption matched, and our previous work indicated that the electromagnetic field enhancement predicted by this model matches experimental measurements, justifying the approximation used.[25] A plane wave, constant wavelength source at 532 nm was utilized. The 3D electromagnetic field was output over several times and normalized against the input source power. The incident wave vector was always perpendicular to the surface. Both the parallel and the perpendicular polarizations were tested. The polarization corresponding to the largest electromagnetic field enhancement was shown in the electromagnetic field visualizations. The visualization was done in the open source MayaVI2 software.

Conflict of Interest: The authors declare no competing financial interest.

Acknowledgment. The resource and facilities used were partially supported by NSF (EPS 1003907), the NASA-WV Space Grant Consortium, the West Virginia University Research Corporation, and the West Virginia EPSCoR Office. A portion of this work was performed in the Biospecimen Processing Core Facility, Mary Babb Randolph Cancer Center, West Virginia University, Morgantown, WV, which is supported in part by NIH Grant P30 GM103488 and P30 RR 032138. The use of WVU shared facility was acknowledged. S.C. is supported by the National Science Foundation Graduate Research Fellowship under Grant No. 1102689. D.M. is grateful for the financial support from the Natural Sciences and Engineering Research Council of Canada and Fonds de la recherche sur la nature et les technologies. W.P. is supported by the Mylan Chair of Pharmacology at the WVU Health Sciences Center. L.G. is supported, in part, by NIH R01 HL056888, NIH RO1 CA134573, the Alexander B. Osborn Hematopoietic Malignancy and Transplantation Program, and the WV Research Trust Fund.

Supporting Information Available: Figures S1−S5 and Table S1. This material is available free of charge *via* the Internet at http://pubs.acs.org.

REFERENCES AND NOTES

1. Arya, S. K.; Bhansali, S. Lung Cancer and Its Early Detection Using Biomarker-Based Biosensors. *Chem. Rev.* **2011**, *111*, 6783–6809.
2. Ai, K.; Zhang, B.; Lu, L. Europium-Based Fluorescence Nanoparticle Sensor for Rapid and Ultrasensitive Detection of an Anthrax Biomarker. *Angew. Chem., Int. Ed.* **2009**, *48*, 304–308.
3. Trantum, J. R.; Wright, D. W.; Haselton, F. R. Biomarker-Mediated Disruption of Coffee-Ring Formation as a Low Resource Diagnostic Indicator. *Langmuir* **2012**, *28*, 2187–2193.
4. Kim, D. M.; Noh, H. B.; Park, D. S.; Ryu, S. H.; Koo, J. S.; Shim, Y. B. Immunosensors for Detection of Annexin II and MUC5AC for Early Diagnosis of Lung Cancer. *Biosens. Bioelectron.* **2009**, *25*, 456–462.
5. Ambrosi, A.; Airò, F.; Merkoçi, A. Enhanced Gold Nanoparticle Based ELISA for a Breast Cancer Biomarker. *Anal. Chem.* **2010**, *82*, 1151–1156.
6. Wang, K. Y.; Chuang, S. A.; Lin, P. C.; Huang, L. S.; Chen, S. H.; Ouarda, S.; Pan, W.-H.; Lee, P. Y.; Lin, C. C.; Chen, Y. J. Multiplexed Immunoassay: Quantitation and Profiling of Serum Biomarkers Using Magnetic Nanoprobes and MALDI-TOF MS. *Anal. Chem.* **2008**, *80*, 6159–6167.
7. DeCaprio, A. P. Biomarkers: Coming of Age for Environmental Health and Risk Assessment. *Environ. Sci. Technol.* **1997**, *31*, 1837–1848.

8. Van Emon, J. M.; Gerlach, C. L. A Status Report on Field-Portable Immunoassay. *Environ. Sci. Technol.* **1995**, *29*, 312A–317A.
9. Rissin, D. M.; Kan, C. W.; Campbell, T. G.; Howes, S. C.; Fournier, D. R.; Song, L.; Piech, T.; Patel, P. P.; Chang, L.; Rivnak, A. J.; *et al.* Single-Molecule Enzyme-Linked Immunosorbent Assay Detects Serum Proteins at Subfemtomolar Concentrations. *Nat. Biotechnol.* **2010**, *28*, 595–599.
10. Rosi, N. L.; Mirkin, C. A. Nanostructures in Biodiagnostics. *Chem. Rev.* **2005**, *105*, 1547–156.
11. Malhotra, R.; Patel, V.; Chikkaveeraiah, B. V.; Munge, B. S.; Cheong, S. C.; Zain, R. B.; Abraham, M. T.; Dey, D. K.; Gutkind, J. S.; Rusling, J. F. Ultrasensitive Detection of Cancer Biomarkers in the Clinic by Use of a Nanostructured Microfluidic Array. *Anal. Chem.* **2012**, *84*, 6249–6255.
12. Zhang, F.; Haushalter, R. C.; Haushalter, R. W.; Shi, Y.; Zhang, Y.; Ding, K.; Zhao, D.; Stucky, G. D. Rare-Earth Upconverting Nanobarcodes for Multiplexed Biological Detection. *Small* **2011**, *7*, 1972–1976.
13. Ranzoni, A.; Sabatte, G.; van IJzendoorn, L. J.; Prins, M. W. J. One-Step Homogeneous Magnetic Nanoparticle Immunoassay for Biomarker Detection Directly in Blood Plasma. *ACS Nano* **2012**, *6*, 3134–3141.
14. Li, Z.; Wang, Y.; Wang, J.; Tang, Z.; Pounds, J. G.; Lin, Y. Rapid and Sensitive Detection of Protein Biomarker Using a Portable Fluorescence Biosensor Based on Quantum Dots and a Lateral Flow Test Strip. *Anal. Chem.* **2010**, *82*, 7008–7014.
15. Reddy, P. J.; Sadhu, S.; Ray, S.; Srivastava, S. Cancer Biomarker Detection by Surface Plasmon Resonance Biosensors. *Clin. Lab. Med.* **2012**, *32*, 47–72.
16. Altintas, Z.; Uludag, Y.; Gurbuz, Y.; Tothill, I. E. Surface Plasmon Resonance Based Immunosensor for the Detection of the Cancer Biomarker Carcinoembryonic Antigen. *Talanta* **2011**, *86*, 377–383.
17. Stern, E.; Vacic, A.; Rajan, N. K.; Criscione, J. M.; Park, J.; Ilic, B. R.; Mooney, D. J.; Reed, M. A.; Fahmy, T. M. Label-Free Biomarker Detection from Whole Blood. *Nat. Nanotechnol.* **2010**, *5*, 138–142.
18. Wang, C.; Ma, L.; Su, M. Simultaneous Detection of Multiple Biomarkers with Several Orders of Concentration Difference Using Phase Change Nanoparticles. *Anal. Chem.* **2011**, *83*, 2215–2219.
19. Wang, C.; Ma, L.; Chen, L.; Chai, K. X.; Su, M. Scanning Calorimetric Detections of Multiple DNA Biomarkers Contained in Complex Fluids Using Phase Change Nanoparticles. *Anal. Chem.* **2010**, *82*, 1838–1843.
20. Li, M.; Zhang, J.; Suri, S.; Sooter, L. J.; Ma, D.; Wu, N. Detection of Adenosine Triphosphate with an Aptamer Biosensor Based on Surface-Enhanced Raman Scattering. *Anal. Chem.* **2012**, *84*, 2837–2842.
21. Chon, H.; Lee, S.; Son, S. W.; Oh, C. H.; Choo, J. Highly Sensitive Immunoassay of Lung Cancer Marker Carcinoembryonic Antigen Using Surface-Enhanced Raman Scattering of Hollow Gold Nanospheres. *Anal. Chem.* **2009**, *81*, 3029–3034.
22. Grubisha, D. S.; Lipert, R. J.; Park, H.-Y.; Driskell, J.; Porter, M. D. Femtomolar Detection of Prostate-Specific Antigen: An Immunoassay Based on Surface-Enhanced Raman Scattering and Immunogold Labels. *Anal. Chem.* **2003**, *75*, 5936–5943.
23. Han, D.; Lim, S. Y.; Kim, B. J.; Piao, L.; Chung, T. D. Mercury(II) Detection by SERS Based on a Single Gold Microshell. *Chem. Commun.* **2010**, *46*, 5587–5589.
24. Barhoumi, A.; Halas, N. J. Label-Free Detection of DNA Hybridization Using Surface Enhanced Raman Spectroscopy. *J. Am. Chem. Soc.* **2010**, *132*, 12792–12793.
25. Li, M.; Cushing, S. K.; Zhang, J.; Lankford, J.; Aguilar, Z. P.; Ma, D.; Wu, N. Shape-Dependent Surface-Enhanced Raman Scattering in Gold–Raman-Probe–Silica Sandwiched Nanoparticles for Biocompatible Applications. *Nanotechnology* **2012**, *23*, 115501.
26. He, S.; Liu, K.-K.; Su, S.; Yan, J.; Mao, X.; Wang, D.; He, Y.; Li, L. J.; Song, S.; Fan, C. Graphene-Based High-Efficiency Surface-Enhanced Raman Scattering-Active Platform for Sensitive and Multiplex DNA Detection. *Anal. Chem.* **2012**, *84*, 4622–4627.
27. Zhang, H.; Harpster, M. H.; Wilson, W. C.; Johnson, P. A. Surface-Enhanced Raman Scattering Detection of DNAs Derived from Virus Genomes Using Au-Coated Paramagnetic Nanoparticles. *Langmuir* **2012**, *28*, 4030–4037.
28. Li, M.; Li, R.; Li, C. M.; Wu, N. Q. Electrochemical and Optical Biosensors Based On Nanomaterials and Nanostructures: Review. *Front. Biosci.* **2011**, *S3*, 1308–1331.
29. Zhu, Z.; Meng, H.; Liu, W.; Liu, X.; Gong, J.; Qiu, X.; Jiang, L.; Wang, D.; Tang, Z. Superstructures and SERS Properties of Gold Nanocrystals with Different Shapes. *Angew. Chem., Int. Ed.* **2011**, *50*, 1593–1596.
30. Kumari, G.; Narayana, C. New Nano Architecture for SERS Applications. *J. Phys. Chem. Lett.* **2012**, *3*, 1130–1135.
31. Baik, S. Y.; Cho, Y. J.; Lim, Y. R.; Im, H. S.; Jang, D. M.; Myung, Y.; Park, J.; Kang, H. S. Charge-Selective Surface-Enhanced Raman Scattering Using Silver and Gold Nanoparticles Deposited on Silicon-Carbon Core–Shell Nanowires. *ACS Nano* **2012**, *6*, 2459–2470.
32. Li, M.; Gou, H.; Al-Ogaidi, I.; Wu, N. Nanostructured Sensors for Detection of Heavy Metals: A Review. *ACS Sustainable Chem. Eng.* **2013**, 10.1021/sc400019a.
33. Haes, A. J.; Haynes, C. L.; McFarland, A. D.; Schatz, G. C.; Van Duyne, R. P.; Zou, S. Plasmonic Materials for Surface-Enhanced Sensing and Spectroscopy. *MRS Bull.* **2005**, *30*, 368–375.
34. Xu, J.; Kvasnička, P.; Idso, M.; Jordan, R. W.; Gong, H.; Homola, J.; Yu, Q. Understanding the Effects of Dielectric Medium, Substrate, and Depth on Electric Fields and SERS of Quasi-3D Plasmonic Nanostructures. *Opt. Express* **2011**, *19*, 20493–20505.
35. Caldwell, J. D.; Glembocki, O.; Bezares, F. J.; Bassim, N. D.; Rendell, R. W.; Feygelson, M.; Ukaegbu, M.; Kasica, R.; Shirey, L.; Hosten, C. Plasmonic Nanopillar Arrays for Large-Area, High-Enhancement Surface-Enhanced Raman Scattering Sensors. *ACS Nano* **2011**, *5*, 4046–4055.
36. Zhang, X.-Y.; Hu, A.; Zhang, T.; Lei, W.; Xue, X.-J.; Zhou, Y.; Duley, W. W. Self-Assembly of Large-Scale and Ultrathin Silver Nanoplate Films with Tunable Plasmon Resonance Properties. *ACS Nano* **2011**, *5*, 9082–9092.
37. Li, M.; Cushing, S. K.; Liang, H.; Suri, S.; Ma, D.; Wu, N. Plasmonic Nanorice Antenna on Triangle Nano-array for Surface-Enhanced Raman Scattering Detection of Hepatitis B Virus DNA. *Anal. Chem.* **2013**, *85*, 2072–2078.
38. Christesen, S. D. Raman Cross-Sections of Chemical-Agents and Simulants. *Appl. Spectrosc.* **1988**, *42*, 318–321.
39. Tarkowski, E.; Issa, R.; Sjögren, M.; Wallin, A.; Blennow, K.; Tarkowski, A.; Kumar, P. Increased Intrathecal Levels of the Angiogenic Factors VEGF and TGF-β in Alzheimer's Disease and Vascular Dementia. *Neurobiol. Aging* **2002**, *23*, 237–243.
40. Ferrara, N. Vascular Endothelial Growth Factor: Basic Science and Clinical Progress. *Endocr. Rev.* **2004**, *25*, 581–611.
41. Storkebaum, E.; Lambrechts, D.; Carmeliet, P. VEGF: Once Regarded as a Specific Angiogenic Factor, Now Implicated in Neuroprotection. *BioEssays* **2004**, *26*, 943–954.
42. Gilfrich, J. V.; Birks, L. S. Estimation of Detection Limits in X-ray Fluorescence Spectrometry. *Anal. Chem.* **1984**, *56*, 77–79.
43. West, S. D.; Turner, L. G. Determination of Spinosad and Its Metabolites in Meat, Milk, Cream, and Eggs by High-Performance Liquid Chromatography with Ultraviolet Detection. *J. Agric. Food Chem.* **1998**, *46*, 4620–4627.
44. Zhou, L.; Ding, F.; Chen, H.; Ding, W.; Zhang, W.; Chou, S. Y. Enhancement of Immunoassay's Fluorescence and Detection Sensitivity Using Three-Dimensional Plasmonic Nano-Antenna-Dots Array. *Anal. Chem.* **2012**, *84*, 4489–4495.
45. Qiu, L. P.; Wang, C. C.; Hu, P.; Wu, Z. S.; Shen, G. L.; Yu, R. Q. A Label-Free Electrochemical Immunoassay for IgG Detection Based on the Electron Transfer. *Talanta* **2010**, *83*, 42–47.
46. Lei, K. F.; Butt, Y. K. Colorimetric Immunoassay Chip Based on Gold Nanoparticles and Gold Enhancement. *Microfluid. Nanofluid.* **2010**, *8*, 131–137.

47. Li, J.; He, X.; Wu, Z.; Wang, K.; Shen, G.; Yu, R. Piezoelectric Immunosensor Based on Magnetic Nanoparticles with Simple Immobilization Procedures. *Anal. Chim. Acta* **2003**, *481*, 191–19842.
48. Zhao, S.; Yang, W.; Lai, R. Y. A Folding-Based Electrochemical Aptasensor for Detection of Vascular Endothelial Growth Factor in Human Whole Blood. *Biosens. Bioelectron.* **2011**, *26*, 2442–2447.
49. Prabhulkar, S.; Alwarappan, S.; Liu, G.; Li, C.-Z. Amperometric Micro-Immunosensor for the Detection of Tumor Biomarker. *Biosens. Bioelectron.* **2009**, *24*, 3524–3530.
50. Suzuki, Y.; Yokoyama, K. Construction of a More Sensitive Fluorescence Sensing Material for the Detection of Vascular Endothelial Growth Factor, a Biomarker for Angiogenesis, Prepared by Combining a Fluorescent Peptide and a Nanopillar Substrate. *Biosens. Bioelectron.* **2011**, *26*, 3696–3699.
51. Pimková, K.; Bocková, M.; Hegnerová, K.; Suttnar, J.; Čermák, J.; Homola, J.; Dyr, J. E. Surface Plasmon Resonance Biosensor for the Detection of VEGFR-1-a Protein Marker of Myelodysplastic Syndromes. *Anal. Bioanal. Chem.* **2012**, *402*, 381–387.
52. Li, H.; Low, J.; Brown, K. S.; Wu, N. Q. Large-Area Well-Ordered Nanodot Array Pattern Fabricated with Self-Assembled Nanosphere Template. *IEEE Sens. J.* **2008**, *8*, 880–884.
53. Li, H.; Wu, N. Q. A Large-Area Nanoscale Gold Hemisphere Pattern as a Nanoelectrode Array. *Nanotechnology* **2008**, *19*, 275301.
54. Oskooi, A. F.; Roundy, D.; Ibanescu, M.; Bermel, P.; Joannopoulos, J. D.; Johnson, S. G. MEEP: A Flexible Free-Software Package for Electromagnetic Simulations by the FDTD Method. *Comput. Phys. Commun.* **2010**, *181*, 687–702.
55. Johnson, P. B.; Christy, R. W. Optical Constants of the Noble Metals. *Phys. Rev. B.* **1972**, *6*, 4370–4379.